Supporting Information

A High-performance Single-active-layer Memristor based on an Ultrananocrystalline Oxygen-deficient TiO_x Film

*Saurabh Srivastava[1], Joseph P. Thomas[1], Nina F. Heinig[1], K. T. Leung[1]**

[1]WATLab and Department of Chemistry, University of Waterloo, Waterloo, Ontario, N2L 3G1, Canada

Corresponding author: K.T.L

*E-mail: tong@uwaterloo.ca

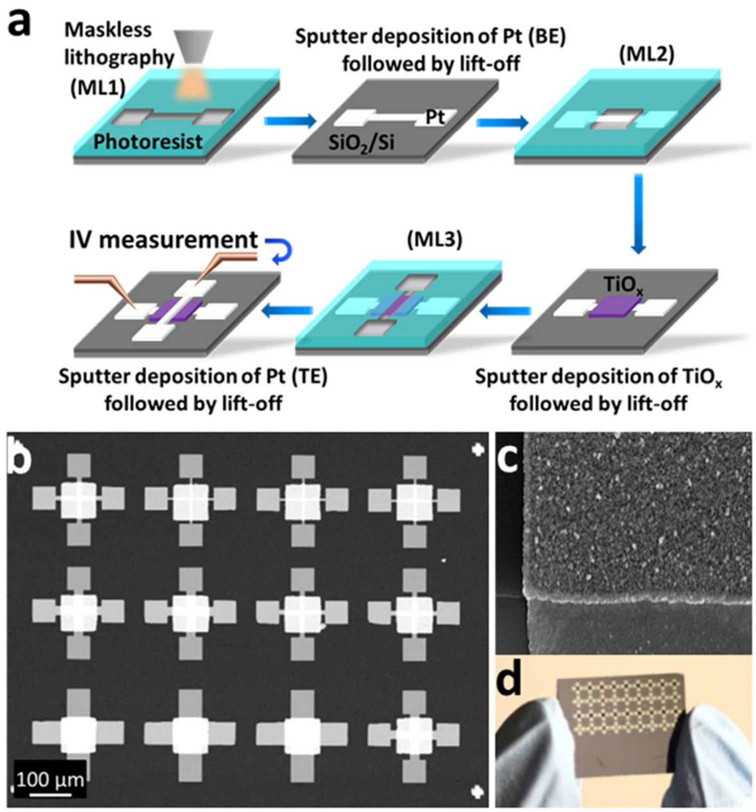

Figure S-1| Device fabrication and electron microscopic analysis. a, Schematic representation of device fabrication involving three maskless lithography (ML) steps. In ML1, an I-bar pattern for the bottom electrode (BE) is exposed to the photoresist. This is then followed by development in MF-24 to remove the photoresist for the pattern, sputter-coating with a 60 nm thick Pt layer, and finally lift-off to remove the remaining photoresist. This process is then repeated in ML2, in which a 60 nm thick TiO_x junction layer is deposited in a square-patterned area, and in ML3, in which a 30 nm thick Pt top electrode (TE) is deposited in an I-bar pattern oriented at right angle to the bottom electrode. Electrical characterization is performed by connecting the microprobes to the top and bottom Pt electrodes to examine the switching process in the TiO_x layer. **b,** SEM image of the array of devices with different junction sizes (5×5 μm^2, 10×10 μm^2, 20×20 μm^2 and 50×50 μm^2) fabricated on the same chip, and **c,** SEM image of selected TiO_x surface morphology at high magnification. **d,** Photograph of the actual device array.

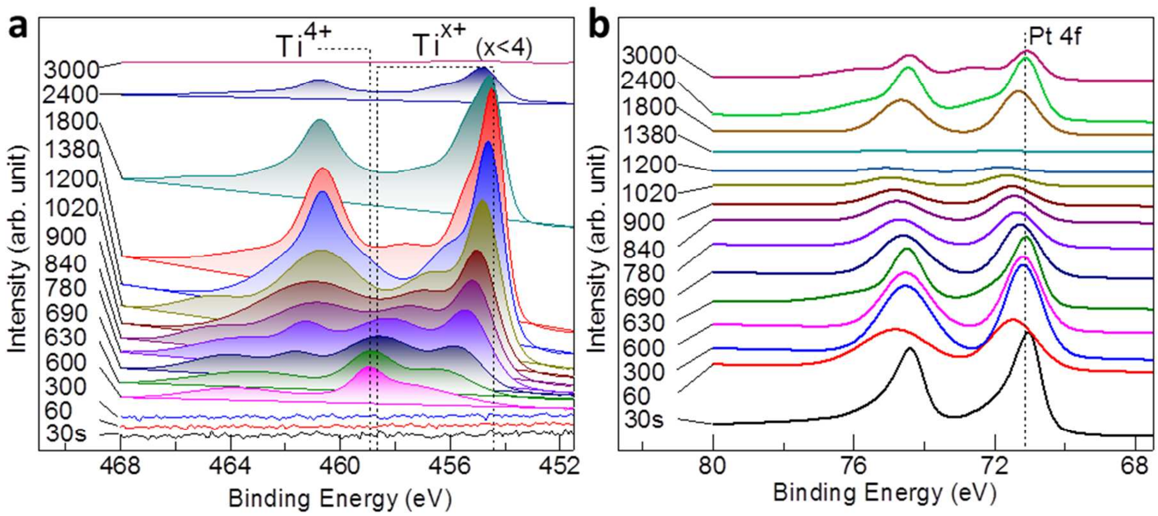

Figure S-2| XPS analysis of the Pt/TiO_x/Pt memristor. Depth-profiling XPS spectra of **a**, Ti 2p and **b,** Pt 4f regions for the memristor device with a Pt/TiO_x/Pt structure. In contrast to Figure 1d that shows the XPS spectra of a TiO_x/Pt structure (i.e., without the top Pt electrode), the presence of the Ti^{n+} features is evident from the very beginning of sputtering the TiO_x layer and after the top Pt layer is removed.

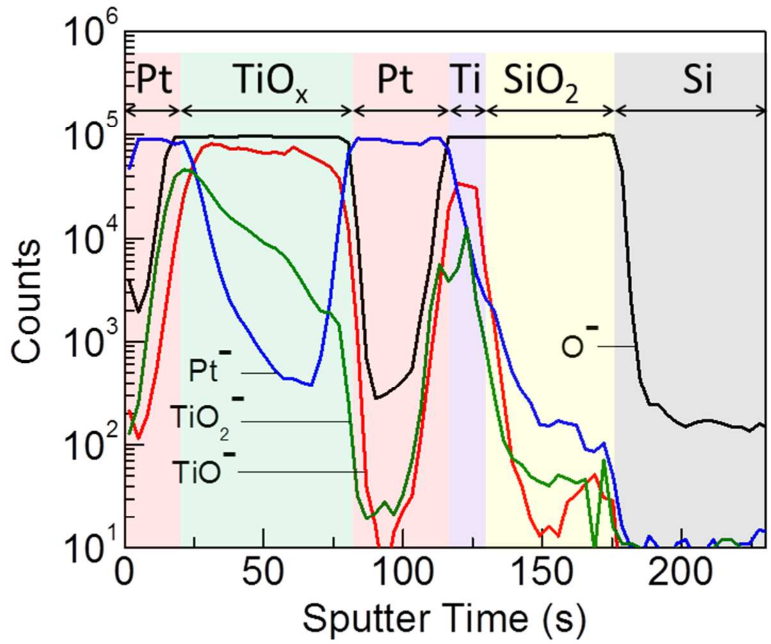

Figure S-3| SIMS depth profiles for the Pt/TiO_x/Pt memristor with a junction size of 50×50 μm^2. Secondary ion mass spectrometry (SIMS) is used to examine the changes in the elemental composition in the multilayer device as a function of sputtering depth, with different layer regions of the device marked by different colors. Evidently, there is a uniform distribution of oxygen within the TiO_x matrix and there is minimal oxygen diffusion into the Pt layer, which accounts for the stability of the electrode.

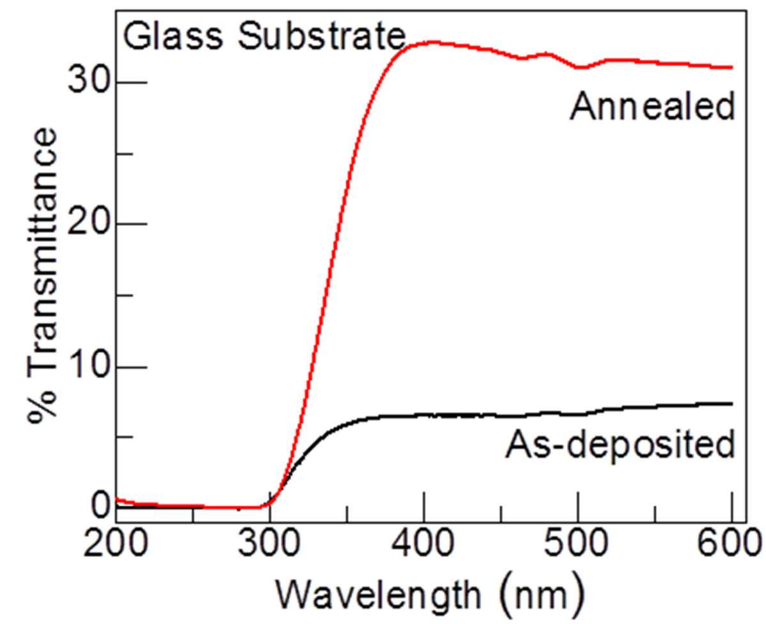

Figure S-4| Optical properties of as-deposited TiO_x film and upon annealed at 600 °C. UV-Vis transmission spectra for the TiO_x film as-deposited and annealed (at 600 °C for 90 min in air) on glass substrates. The difference in the transmittance is due to the change to a more stoichiometric TiO_2 phase as a result of oxidation in the annealing step. The as-deposited film is semi-transparent with the observed transmittance at ~8%, while annealing causes the sample to become more transparent, with the transmittance increased to ~30%. This can be correlated with the phase change from TiO_x to TiO_2 phase due to oxidation during annealing.

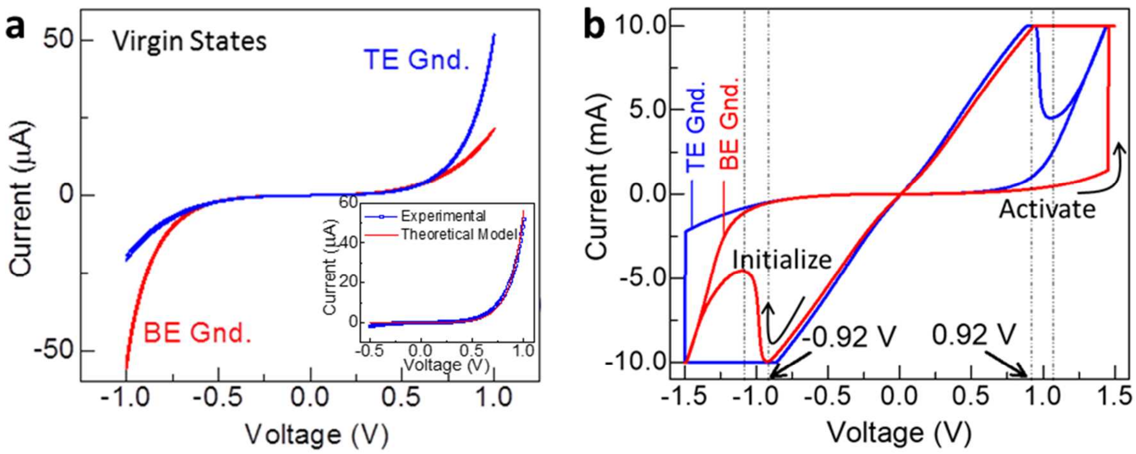

Figure S-5| Virgin and activation states of the memristor device with a 50×50 μm^2 junction size. a, In the virgin state, the I-V curve is obtained with a sweep voltage (±1.0 V) applied on either of the top or bottom electrodes while keeping the respective other electrode grounded. Because of the single-phase TiO_x film, this interface-type switching behavior is irrespective of the directional bias, i.e. the I-V curve obtained with the bias applied on the top electrode (TE) [and the bottom electrode (BE) grounded] is a mirror image of that obtained with the bias applied on the bottom electrode (and the top electrode grounded). Inset compares the experimental IV curve for the virgin state with theoretical data obtained from the Schottky barrier equation for the thermionic emission model.[9,17] **b,** During the device activation step, resistive switching is obtained at an activation voltage of +1.5 V and –1.5 V for the device operated with BE and TE grounded, respectively. The corresponding I-V behavior also exhibits a negative differential resistance region starting at –0.92 V and +0.92 V, respectively. The similar resistive switching behavior of the device found when operated with both directions of the applied bias reveals the similar nature of the top Pt/TiO_x and the bottom TiO_x/Pt interfaces.

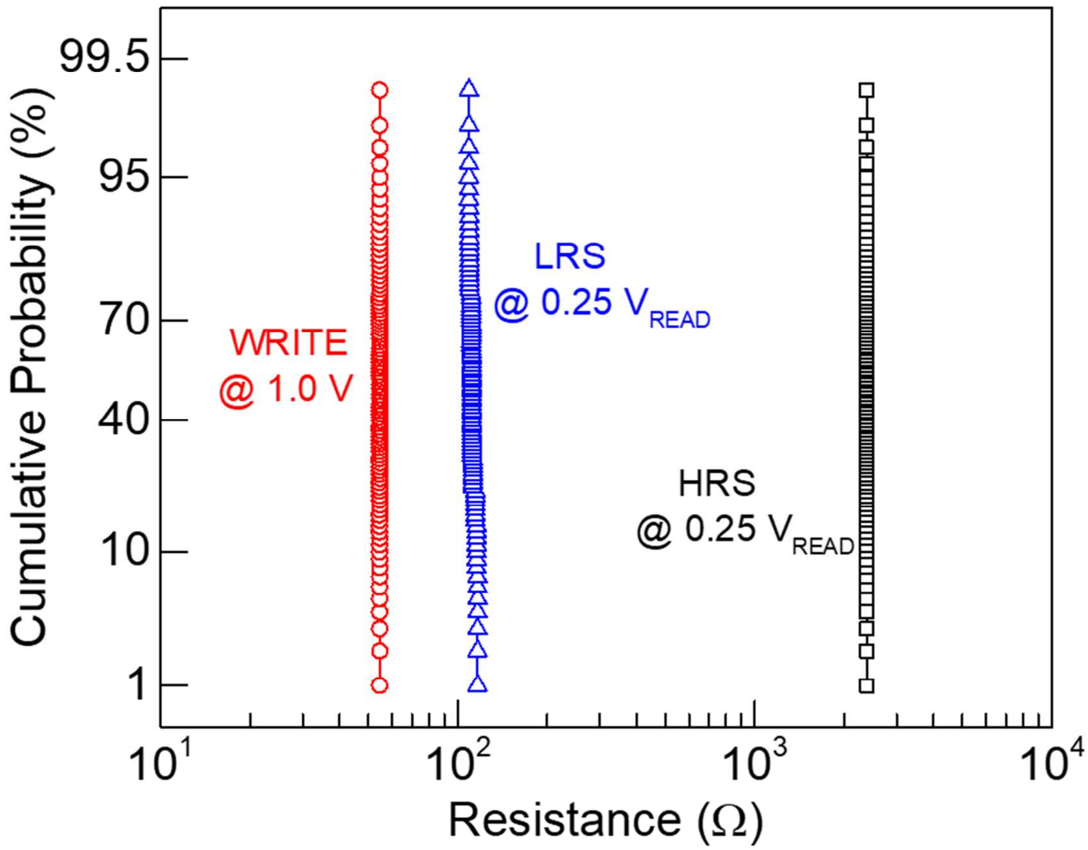

Figure S-6| Cumulative probability distribution plots. The cumulative probability distributions of the resistance levels of the HRS and LRS at a small READ voltage of +0.25 V and the WRITE operation performed at +1.0 V. The extremely narrow distributions suggest the exceptional uniformity of the resistance states of the device.

Table S1| Comparison of various memristor device architectures with single layer and multilayer switching matrices and their respective electroforming and SET/RESET voltages.*

Device Structure	Electroforming/ Activation voltage	SET/RESET Voltage	Reference
Single-layer matrix			
AFM Tip/$SrTiO_3$/Pt-Au	-5 V	±4 V	Szot et al. (2006) [1]
Pt/TiO_2/Pt	NA	2/3 V	Kwon et al. (2010) [2]
Pt/TiO_2/Pt	-6 V	±0.6	Strachan et al. (2011) [3]
Pt/Ta_2O_5/Pt	-10 V	+0.6/-0.8 V	Strachan et al. (2011) [4]
Ti-Pt/TiO_2/Au-pt	-14 V	+3/+2.5 V	Strukov et al. (2012) [5]
ZnO Nanorods	4 V	±2 V	Park et al. (2013) [6]
Pt/TiO_2/Pt	-8 V	±4 V	Jiang et al. (2013) [7]
Pt/TiO_2/Pt	Forming-free	+3.6/-4 V	Salaoru et al. (2013) [8]
Au NP/$SrTiO_3$ interface	10 V	4/-6 V	Hou et al.(2014) [9]
TaO_x, HfO_x, TiO_x	-5 V	±2 V	Wedig et al. (2015) [10]
Pt/TiO_x/Pt	+1.5 V	+0.59 V	**This work**
Multilayer Matrix			
Pt/Ta_2O_{5-x}/TaO_{2-x}/Pt	-3 V	-1/+2 V	Lee et al. (2011) [11]
Pt/TiO_x/TiO_y/TiO_x/Pt	-10 V	±1.5 V	Bae et al. (2012) [12]
Pt/Ta_2O_5/HfO_{2-x}/TiN	-10 V	±3-4 V	Yoon et al. (2014) [13]
Pd/Si:Ta_2O_{5-x}/TaO_y/Pd	4-10 V	-1-1.5 V	Kim et al. (2014) [14]
Pt/Nb-$SrTiO_3$-Sm_2O_3 interface	Forming-free	10 V	Lee et al. (2014) [15]
Pt/HfO_2/Hf/Pt	2.5 V	±1.5 V	Breuer et al. (2015) [16]
Ag/MoO_x/MoS_2/Ag	Forming-free	±0.2 V	Bessonov et al. (2015) [17]
Ta/TaO_x/TiO_2/Ti	Forming-free	±6 V	Wang et al. (2015) [18]
Au/$BaTiO_3$/NiO/Pt	+6 V	±1 V	Li et al. (2016) [19]

*Our device shows the best performance among the devices with single-layer switching matrix and is also better than most of the devices with multilayer switching matrices. While the multilayer devices by Bessonov et al. have shown better performance than the present single-active-layer device, their devices have potentially shorter lifetime because of the oxidation prone silver nanowire in ambient, in addition to an apparently more complex fabrication process. Like most devices that require electroforming, their devices are also unidirectional.

References:

(1) Szot, K.; Speier, W.; Bihlmayer, G.; Waser, R. Switching the Electrical Resistance of Individual Dislocations in Single-Crystalline $SrTiO_3$. *Nat. Mater.* **2006**, *5* (4), 312–320.

(2) Kwon, D. H.; Kim, K. M.; Jang, J. H.; Jeon, J. M.; Lee, M. H.; Kim, G. H.; Li, X. S.; Park, G. S.; Lee, B.; Han, S.; Kim, M.; Hwang, C. S. Atomic Structure of Conducting Nanofilaments in TiO_2 Resistive Switching Memory. *Nat. Nanotechnol.* **2010**, *5* (2), 148–153.

(3) Strachan, J. P.; Strukov, D. B.; Borghetti, J.; Yang, J. J.; Medeiros-Ribeiro, G.; Williams, R. S. The Switching Location of a Bipolar Memristor: Chemical, Thermal and Structural Mapping. *Nanotechnology* **2011**, *22* (25), 254015.

(4) Strachan, J. P.; Medeiros-Ribeiro, G.; Yang, J. J.; Zhang, M.; Miao, F.; Goldfarb, I.; Holt, M.; Rose, V.; Williams, R. S. Spectromicroscopy of Tantalum Oxide Memristors. *Appl. Phys. Lett.* **2011**, *98*, 242114 (1-3).

(5) Strukov, D. B.; Alibart, F.; Williams, R. S. Thermophoresis/diffusion as a Plausible Mechanism for Unipolar Resistive Switching in Metal-Oxide-Metal Memristors. *Appl. Phys. A Mater. Sci. Process.* **2012**, *107* (3), 509–518.

(6) Park, J.; Lee, S.; Lee, J.; Yong, K. A Light Incident Angle Switchable ZnO Nanorod Memristor: Reversible Switching Behavior between Two Non-Volatile Memory Devices. *Adv. Mater.* **2013**, *25* (44), 6423–6429.

(7) Jiang, H.; Xia, Q. Effect of Voltage Polarity and Amplitude on Electroforming of TiO_2 Based Memristive Devices. *Nanoscale* **2013**, *5* (8), 3257–3261.

(8) Salaoru, I.; Khiat, A.; Li, Q.; Berdan, R.; Prodromakis, T. Pulse-Induced Resistive and Capacitive Switching in TiO_2 Thin Film Devices. *Appl. Phys. Lett.* **2013**, *103* (23), 233513 (1-4).

(9) Hou, J.; Nonnenmann, S. S.; Qin, W.; Bonnell, D. A. Size Dependence of Resistive Switching at Nanoscale Metal-Oxide Interfaces. *Adv. Funct. Mater.* **2014**, *24* (100), 4113–4118.

(10) Wedig, A.; Luebben, M.; Moors, M.; Cho, D. Y.; Skaja, K.; Hasegawa, T.; Adepalli, K. K.; Yildiz, B.; Waser, R.; Valov, I. Nanoscale Cation Motion in TaO_x, HfO_x and TiO_x Memristive Systems. *Nat. Nanotechnol.* **2015**, *11* (September), 67–75.

(11) Lee, M. J.; Lee, C. B.; Lee, D.; Lee, S. R.; Chang, M.; Hur, J. H.; Kim, Y. B.; Kim, C. J.; Seo, D. H.; Seo, S.; Chung, U. I.; Yoo, I. K.; Kim, K. A Fast, High-Endurance and Scalable Non-Volatile Memory Device Made from Asymmetric Ta_2O_{5-x}/TaO_{2-x} Bilayer Structures. *Nat. Mater.* **2011**, *10* (8), 625–630.

(12) Bae, Y. C.; Lee, A. R.; Lee, J. B.; Koo, J. H.; Kwon, K. C.; Park, J. G.; Im, H. S.; Hong, J.

P. Oxygen Ion Drift-Induced Complementary Resistive Switching in Homo $TiO_x/TiO_y/TiO_x$ and Hetero TiO_x/TiON/TiO_x Triple Multilayer Frameworks. *Adv. Funct. Mater.* **2012**, *22* (4), 709–716.

(13) Yoon, J. H.; Song, S. J.; Yoo, I. H.; Seok, J. Y.; Yoon, K. J.; Kwon, D. E.; Park, T. H.; Hwang, C. S. Highly Uniform, Electroforming-Free, and Self-Rectifying Resistive Memory in the Pt/Ta_2O_5/HfO_{2-x}/TiN Structure. *Adv. Funct. Mater.* **2014**, *24* (32), 5086–5095.

(14) Kim, S.; Choi, S.; Lee, J.; Lu, W. D. Tuning Resistive Switching Characteristics of Tantalum Oxide Memristors through Si Doping. *ACS Nano* **2014**, *8* (10), 10262–10269.

(15) Lee, S.; Sangle, A.; Lu, P.; Chen, A.; Zhang, W.; Lee, J. S.; Wang, H.; Jia, Q.; Macmanus-driscoll, J. L. Novel Electroforming-Free Nanoscaffold Memristor with Very High Uniformity, Tunability, and Density. *Adv. Mater.* **2014**, *26*, 6284–6289.

(16) Breuer, T.; Siemon, A.; Linn, E.; Menzel, S.; Waser, R.; Rana, V. A HfO_2-Based Complementary Switching Crossbar Adder. *Adv. Electron. Mater.* **2015**, *1*, 1500138 (1-10).

(17) Bessonov, A. A.; Kirikova, M. N.; Petukhov, D. I.; Allen, M.; Ryhänen, T.; Bailey, M. J. A. Layered Memristive and Memcapacitive Switches for Printable Electronics. *Nat. Mater.* **2015**, *14*, 199–204.

(18) Wang, Y.-F.; Lin, Y.-C.; Wang, I.-T.; Lin, T.-P.; Hou, T.-H. Characterization and Modeling of Nonfilamentary Ta/TaO_x/TiO_2/Ti Analog Synaptic Device. *Sci. Rep.* **2015**, *5*, 10150.

(19) Li, S.; Wei, X.; Lei, Y.; Yuan, X.; Zeng, H. Complementary Resistive Switching in $BaTiO_3$/NiO Bilayer with Opposite Switching Polarities. *Appl. Surf. Sci.* **2016**, *389*, 977–982.